Chapter 3 - ZrTi Based Be Bearing Glasses Optimized for High Thermal Stability and Thermoplastic Formability

We flesh out the details of the alloy development story in this chapter with a thorough exploration of the ZrTiBe system and the large ΔT quaternary compositions. This chapter draws heavily on the article "ZrTi based Be bearing glasses optimized for high thermal stability and thermoplastic formability" published in Acta Materialia [A. Wiest, G. Duan, M.D. Demetriou, L.A. Wiest, A. Peck, G. Kaltenboeck, B. Wiest, W.L. Johnson, Acta Mater. 56 (2008) 2625].

A new class of ZrTi based Be bearing (Vitreloy) glass forming compositions that exhibit high thermal stability and good glass forming ability is reported. Optimized ternary compositions were obtained by reexamining the ZrTiBe phase diagram for regions that produce glasses having high thermal stability and modest glass forming ability. By incorporating a fourth element in the optimized ternary compositions, quaternary alloys were obtained having thermal stabilities twice that of $Zr_{41.2}Ti_{13.8}Ni_{10}Cu_{12.5}Be_{22.5}$ (Vitreloy 1) while exhibiting good glass forming abilities. Optimized quaternary alloys exhibiting critical casting thicknesses exceeding 15mm and thermal stabilities as high as 165 ºC are reported herein. The good thermal stability of these alloys renders them attractive for forming processes that can be performed thermoplastically in the supercooled liquid region, in a manner similar to the forming of polymers.

3.1 Introduction

Over the last decade, families of bulk glass forming metallic systems exhibiting remarkable glass forming ability (GFA) have been discovered [1-3]. These relatively

new materials are known to exhibit attractive mechanical properties, including high (near theoretical) yield strengths, high elastic limits, and good wear resistance. More interestingly, the ability of amorphous metals to soften and flow upon relaxation at the glass transition gives rise to a viscoplastic flow behavior enabling unique forming capabilities that resemble those of plastics and conventional glasses [4-6]. Essentially, such thermoplastic forming ability arises as a result of the supercooled liquid thermal stability and fragility.

The liquid thermal stability can be defined as the resistance of a glassy sample to crystallize upon heating above the glass transition temperature, T_g, and is typically quantified by the temperature region bounded between T_g and T_x, i.e., $\Delta T = T_g - T_x$, where T_x is the temperature at which a sample crystallizes at a certain heating rate. This temperature region is typically referred to as the supercooled liquid region (SCLR). The glass fragility (m) is referred to as the steepness of the equilibrium temperature dependent viscosity at T_g [7]. Given that the viscosity of liquids is a hyper-Arrhenius function of temperature, one can reasonably assume that the higher the m and ΔT for a given glass, the lower the accessible viscosities in the SCLR that could be utilized for forming.

Many forming processes have been attempted with metallic glasses in the SCLR. Micro and nano replication [8-9], powder consolidation [10], extrusion [11], and recently blow molding [12] have been demonstrated. These processes are collectively referred to as thermoplastic forming processes. The success and feasibility of these and similar processes are dependant on the processing time available at the accessible viscosities in the SCLR. Very few alloys are known to exhibit the combination of thermal stability and fragility necessary for successful thermoplastic forming. The most commonly used

alloys in thermoplastic forming applications are the fragile $Pd_{43}Ni_{10}Cu_{27}P_{20}$ and $Pt_{57.5}Ni_{5.3}Cu_{14.7}P_{22.5}$ glasses and the thermally stable $Zr_{44}Ti_{11}Cu_{10}Ni_{10}Be_{25}$ (Vitreloy 1b), but even these alloys require high pressures and undergo only limited thermoplastic strains due to the high viscosities and limited processing times available.

In the present work, optimization of ZrTi based Be bearing glasses for large thermal stability is attempted. Measurement of the liquid fragility of these alloys will be the subject of future investigation. Several quaternary ZrTi based Be bearing glasses with high ΔT and good GFA will be presented. The alloy optimization was approached by examining the ternary ZrTiBe system for compositions exhibiting large ΔT and modest GFA. Some of the ternary compositions investigated here for bulk glass forming ability include those investigated previously by Tanner [13], who focused primarily on their amorphous ribbon forming ability. An appropriate fourth "solute element" at an optimum fraction was added to the ternary compositions, and in most cases, both ΔT and glass forming were seen to increase until too high a concentration of solute precipitated additional phases. Late transition metals were found to be the optimum solute element. Ni was not considered a viable solute atom as ample evidence in the literature suggests that the NiTi rich quasicrystal is the first phase to nucleate in Vitreloy glasses, providing nucleation sites for other crystals that eventually crystallize the alloy [14-15]. This is the approach that led to the development of the recently reported $Zr_{35}Ti_{30}Cu_{8.25}Be_{26.75}$ alloy [16], having $\Delta T = 159$ °C and a processing viscosity prior to crystallization of $\sim 10^4$ Pa-s.

3.2 Experimental Method

Alloys were prepared using elements of >99.9% purity. The elements were weighed to within ± 0.1% of the calculated mass to ensure accurate compositions, and

were ultrasonically cleaned in acetone and ethanol prior to melting. Typically 6 g ingots were arc melted on a Cu plate in a Ti-gettered argon atmosphere and flipped at least three times to ensure chemical homogeneity. The mass was again measured after melting to ensure proper composition, and alloys with greater than ± 0.1% deviation from the originally weighed mass were discarded.

Rods were cast under an argon atmosphere using an Edmund Buhler mini arc melter suction casting setup or by injecting inductively molten alloy from quartz nozzles into a copper mold. The largest diameter rod for which each alloy casts fully amorphous is reported as critical casting thickness or GFA. The amorphous nature of the rods was verified using a Philips X'Pert Pro X-ray Diffractometer and thermodynamic data was collected in graphite crucibles at 20 K/min using a Netzsch 404C Pegasus Differential Scanning Calorimeter (DSC). T_g, T_x, solidus temperature (T_s), liquidus temperature (T_L) and enthalpy of crystallization (ΔH_x) are reported.

Casting techniques introduced a large variability into the DSC results. Thermodynamic data is reported from DSC scans of mini arc melter cast specimens. For different segments of a mini arc melter cast rod (top, middle, bottom), there was less than 3 °C variation in T_g, T_x, T_s, and T_L, while ΔH_x showed less than 5% variability. Variability between rods of the same alloy cast using identical casting methods was also minimal. Critical casting measurements necessitated the use of die casting into large diameter copper molds. Die casting from quartz nozzles into copper molds occasionally lowered the T_x value by as much as 10 °C and larger diameter rods were seen to have lower T_g values than smaller diameter rods. Error bars are ± 3 °C on temperatures and ± 5% on ΔH_x.

3.3 Results and Discussion

The ZrTiBe system was investigated in the 1970s by Tanner, who discovered that amorphous ribbons (10-100μm thick) could be produced by means of melt spinning at cooling rates of 10^5 - 10^6 K/s [17]. Ternary phase diagrams showing isothermal sections of the composition space are published, but very little of the thermodynamic data on the glasses is available [18].

In this study, many of the alloys reported to be glassy ribbons were recreated, primarily those in the low melting temperature regions given by the isothermal cross section phase diagrams. Several bulk glasses with critical casting thicknesses between 1mm and 6mm were identified from those compositions. Bulk GFA regions are shown in Figure 3.1. The ternary phase diagram showing the Tanner glassy ribbons region is presented in Figure 3.2. Twenty-two bulk glass forming compositions are outlined in the diagram. The thermodynamic data for these compositions are listed in Table 3.1.

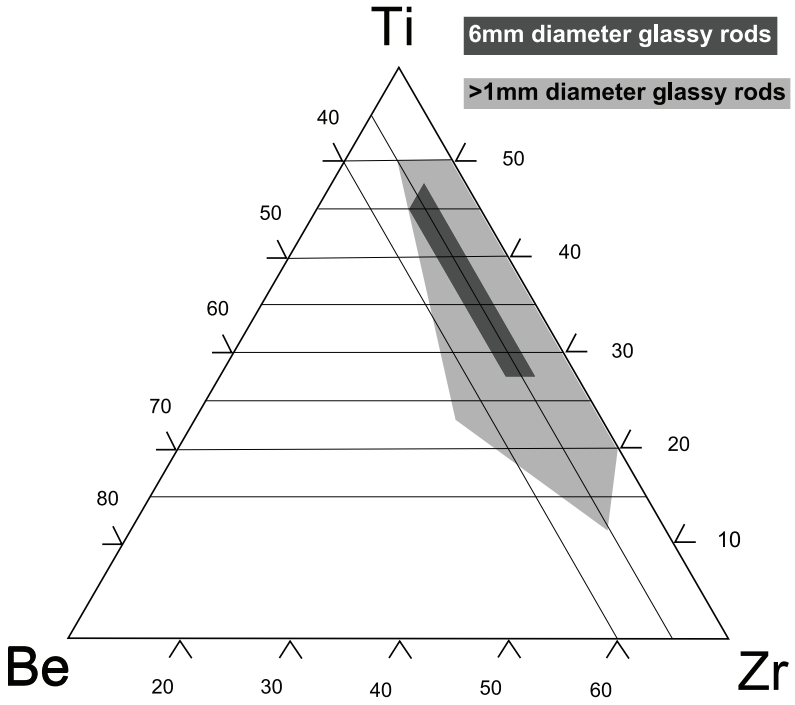

Figure 3.1: Bulk glass forming regions shown on ZrTiBe phase diagram.

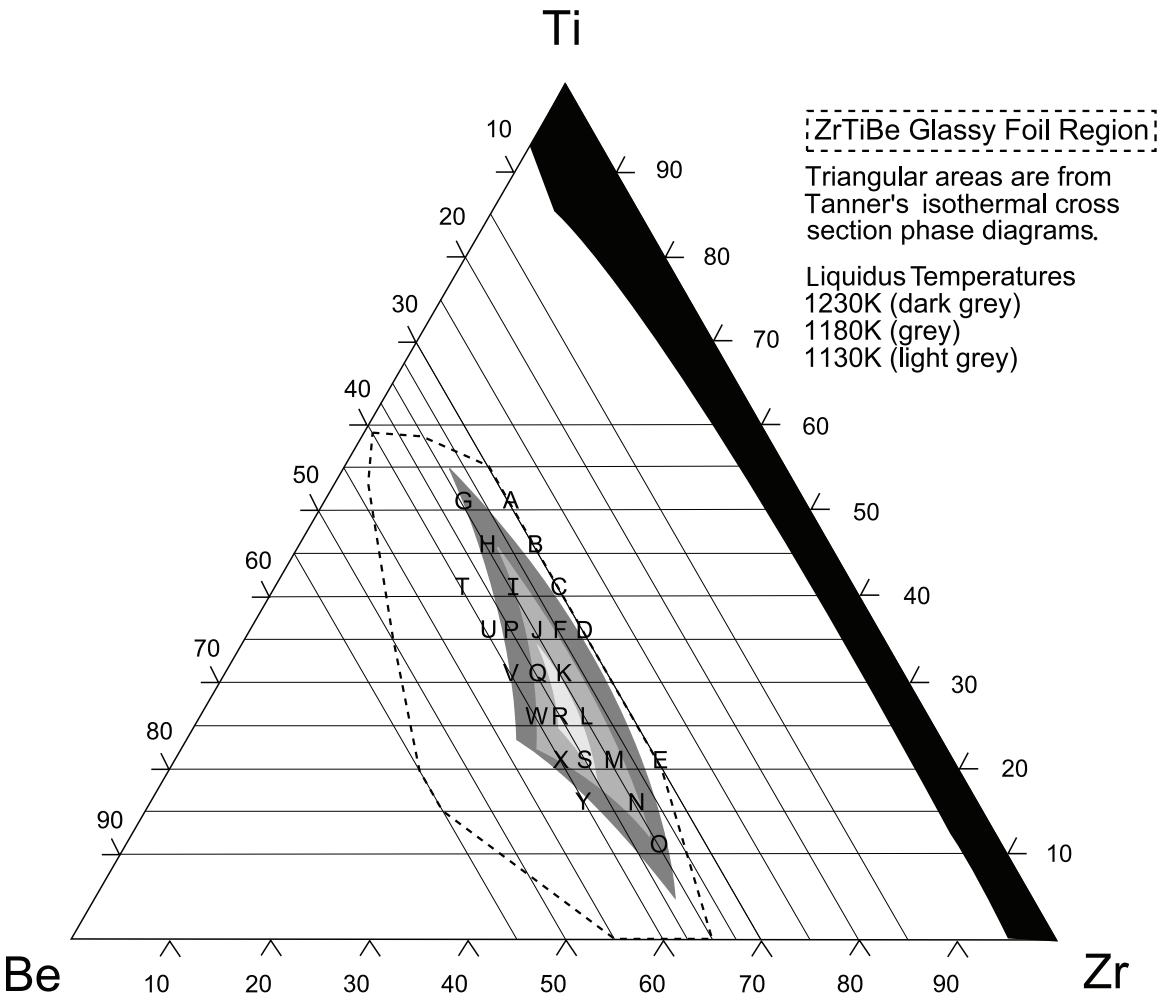

Figure 3.2: Ternary ZrTiBe phase diagram showing the region originally explored by Tanner for ribbon forming glasses (dashed line), the isothermal cross sections showing the liquid phase at various temperatures (shaded triangles), and the alloys recreated in this experiment (letters).

Alloys H, I, J and K are found to have a critical casting thickness of 6mm [19]. This is rather surprising, considering the extensive investigation previously performed in this system. The work of Peker and Johnson [20] indicates that addition of at least one late transition metal was necessary to form a bulk glass in this system. Tanner on the other hand, explored the ZrTiBe system and concluded that glass formation required cooling rates of $10^5 - 10^6$ K/s, which limited the dimension of amorphous samples to ~ 100μm thick. The presence of bulk glass formers in the ternary system facilitated the

optimization of quaternary alloys for large ΔT by allowing a large range of additional elements to be added without concern for GFA.

Table 3.1: Thermodynamic data of the alloys listed in Figure 3.2.

Alloy	Composition	T_g [C]	T_{x1} [C]	T_{x2} [C]	ΔT	ΔH_x [J/mol]	T_s [C]	T_L [C]	GFA
A	$Zr_{20}Ti_{50}Be_{30}$	288.2	331.4	464.9	43.2	5610	829	>950	>1mm
B	$Zr_{25}Ti_{45}Be_{30}$	308	348.1	454.2	40.1	4121	846	850.2	>1mm
C	$Zr_{30}Ti_{40}Be_{30}$	293.7	339.2	439.5	45.5	6177	838	848.9	>1mm
D	$Zr_{35}Ti_{35}Be_{30}$	292.2	349	431.3	56.8	6244	842	853.5	>1mm
E	$Zr_{50}Ti_{20}Be_{30}$	292.3	362.9	422.3	70.6	6003	881	>900	>1mm
F	$Zr_{32.5}Ti_{35}Be_{32.5}$	299.4	378.5	444.6	79.1	6477	870	922.1	>1mm
G	$Zr_{15}Ti_{50}Be_{35}$	313.4	366.1	503.2	52.7	5484	830	914.5	>0.5mm
H	$Zr_{20}Ti_{45}Be_{35}$	319.9	380.5	481.2	60.6	6265	836	848.5	6mm
I	$Zr_{25}Ti_{40}Be_{35}$	322.3	401.7	469.8	79.4	6690	845	850.6	6mm
J	$Zr_{30}Ti_{35}Be_{35}$	308	412.8	454	105	6964	838	845	6mm
K	$Zr_{35}Ti_{30}Be_{35}$	319	439.2	-	120	6284	849	861.5	6mm
L	$Zr_{40}Ti_{25}Be_{35}$	300.2	409	429	109	5796	838	934.3	>1mm
M	$Zr_{45}Ti_{20}Be_{35}$	304.7	402.7	423.4	98	6421	877	>950	>1mm
N	$Zr_{50}Ti_{15}Be_{35}$	302.4	398	418	95.6	6613	879	>950	>1mm
O	$Zr_{55}Ti_{10}Be_{35}$	306.9	389.4	415.1	82.5	6747	905	>950	>0.5mm
P	$Zr_{27.5}Ti_{35}Be_{37.5}$	317.4	440.2	456.5	123	7167	833	843	>1mm
Q	$Zr_{32.5}Ti_{30}Be_{37.5}$	314.2	427.5	441.8	113	6469	837	846.8	>1mm
R	$Zr_{37.5}Ti_{25}Be_{37.5}$	314.1	413.2	431.4	99.1	6800	831	857.7	>1mm
S	$Zr_{42.5}Ti_{20}Be_{37.5}$	314.8	405.4	424.4	90.6	6382	845	880.8	>1mm
T	$Zr_{20}Ti_{40}Be_{40}$	314.3	433.2	488.8	119	6542	829	853	>0.5mm
U	$Zr_{25}Ti_{35}Be_{40}$	322.2	444.7	449.6	123	7104	831	842.8	>1mm
V	$Zr_{30}Ti_{30}Be_{40}$	330.1	447.4	-	117	6659	826	844.1	>1mm
W	$Zr_{35}Ti_{25}Be_{40}$	325.5	432.4	-	107	6422	837	850	>1mm
X	$Zr_{40}Ti_{20}Be_{40}$	324.8	415.9	-	91.1	6323	842	907.2	>1mm
Y	$Zr_{45}Ti_{15}Be_{40}$	326.4	411.8	-	85.4	7242	880	>900	>1mm

Error bars are ± 3 °C on temperatures and ± 5% on ΔH_x.

Many alloys with large ΔT are found in the ternary system. The 20 K/min DSC scans of some of the ternary alloys are shown in Figure 3.3. It is interesting to note that the scans of the alloys of Figure 3.3 reveal a single exothermic peak following the glass transition, suggesting that these alloys tend to crystallize by simultaneous crystal growth. Many other alloys revealed a small additional exothermic event before or after the main

crystallization event indicating that for these alloys the crystallization was nearly simultaneous. It was found that replacing small fractions of Be with certain late transition metals in alloys that exhibited simultaneous or nearly simultaneous crystal growth had the most beneficial effect on increasing the thermal stability of the alloys.

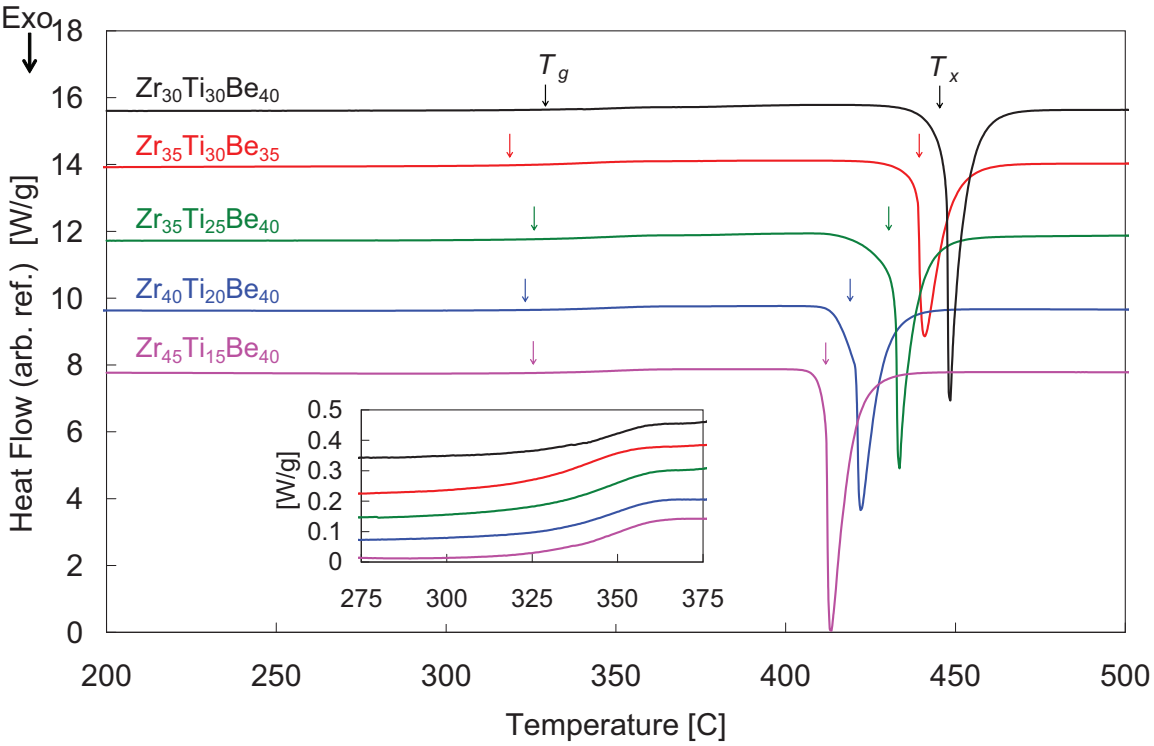

Figure 3.3: 20 K/min DSC scans of several alloys in the ternary ZrTiBe system. Crystallization is seen as a single exothermic peak suggesting that these alloys tend to crystallize by simultaneous crystal growth at that heating rate. Inset: Magnified view of glass transitions (temperature axes aligned); vertical order of alloys maintained.

3.3.1 Quaternary Alloys

Quaternary variants of $Zr_{35}Ti_{30}Be_{35}$ (Alloy K) were most thoroughly investigated because alloy K is in the best glass forming region and has the largest ΔT while still exhibiting simultaneous crystal growth in a 20 K/min DSC scan. Al, Fe, Co, and Cu were substituted for Be and the effect on ΔT was monitored. An increasing ΔT resulted from additions of Fe, Co, and Cu until too high a concentration was reached. Table 3.2

lists the compositions and thermodynamic data for quaternary variants of Alloy K. Figure 3.4 presents 20 K/min DSC scans showing the effect on thermal stability of various additions of Cu, Co, and Fe.

Table 3.2: Thermodynamic data for quaternary variants of $Zr_{35}Ti_{30}Be_{35}$ (Alloy K) obtained by substituting Cu, Co, Fe, Al for Be.

	T_g[C]	T_{x1}[C]	T_{x2}[C]	ΔT	ΔH_x (J/mol)	T_s[C]	T_L[C]	GFA
$Zr_{35}Ti_{30}Be_{35}$ (Alloy K)	319	439.2	-	120.2	6284	848.6	861.5	6mm
$Zr_{35}Ti_{30}Be_{30}Cu_5$	301.7	452.1	-	150.4	7549	674.5	841.2	>10mm
$Zr_{35}Ti_{30}Be_{27.5}Cu_{7.5}$	301.4	466.5	-	165.1	7446	674.4	797.5	>15mm
$Zr_{35}Ti_{30}Be_{26.75}Cu_{8.25}$	305	464	-	159	7444	674	771	>15mm
$Zr_{35}Ti_{30}Be_{25}Cu_{10}$	305.3	426.4	460.1	121.1	7449	672.4	756.7	>10mm
$Zr_{35}Ti_{30}Be_{33}Co_2$	311.1	447.8	-	136.7	7046	729	824.1	>3mm
$Zr_{35}Ti_{30}Be_{31}Co_4$	315.5	467.2	-	151.7	7418	724.7	801.9	>3mm
$Zr_{35}Ti_{30}Be_{29}Co_6$	324.1	476.2	-	152.1	7457	721.7	837.3	>15mm
$Zr_{35}Ti_{30}Be_{27.5}Co_{7.5}$	318.9	407.9	454.8	89	6154	717.8	813.7	>10mm
$Zr_{35}Ti_{30}Be_{33}Fe_2$	312.8	449.6	-	136.8	6796	770.6	827.6	>3mm
$Zr_{35}Ti_{30}Be_{31}Fe_4$	318.5	464.6	-	146.1	6297	759.4	800.5	>3mm
$Zr_{35}Ti_{30}Be_{29}Fe_6$	323.4	451.7	-	128.3	5810	747.8	842.8	>10mm
$Zr_{35}Ti_{30}Be_{27.5}Fe_{7.5}$	328.9	405.6	433.6	76.7	5370	758.2	817.8	>3mm
$Zr_{35}Ti_{30}Be_{30}Al_5$	329.3	459.6	-	130.3	6126	829.8	864.8	>3mm

Error bars are ± 3 °C on temperatures and ± 5% on ΔH_x.

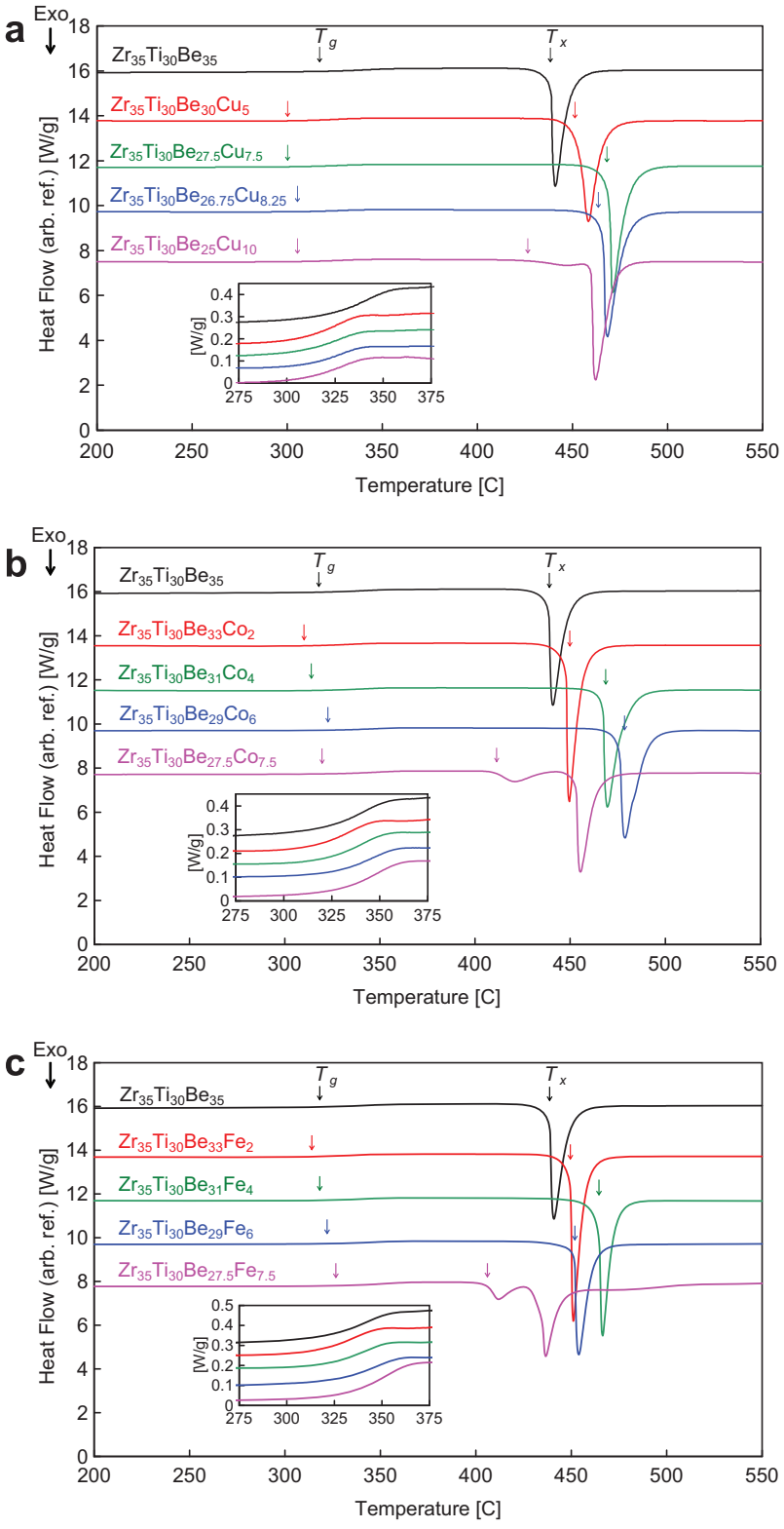

Figure 3.4: (a) The effect of Cu substitution for Be in $Zr_{35}Ti_{30}Be_{35}$ (Alloy K). (b) The effect of Co substitution for Be in $Zr_{35}Ti_{30}Be_{35}$ (Alloy K). (c) The effect of Fe substitution for Be in $Zr_{35}Ti_{30}Be_{35}$ (Alloy K). All insets contain magnified view of glass transitions (temperature axes aligned) with vertical order of alloys maintained.

The largest ΔT values for quaternary variants of alloy K were obtained by substituting Cu for beryllium (Figure 3.4a). The ΔT value peaks at 165.1 °C for the alloy that has 7.5 atomic percent Cu. Co and Fe also increased ΔT significantly, but Fe addition in alloy K was not as beneficial in terms of GFA. Since Cu was observed to have the greatest effect on GFA and ΔT, Cu substitution for Be was performed in many of the large ΔT ternary alloys near alloy K. Table 3.3 presents several examples of such quaternary alloys along with their thermodynamic data.

From Figure 3.4 and Tables 3.2 and 3.3 one can observe that there is an optimal late transition metal substitution for Be for each quaternary family. Substitutions smaller than optimal are shown to have a limited effect on GFA and minimally increase thermal stability, while substitutions larger than optimal tend to precipitate additional phases diminishing ΔT. A summary of the alloys exhibiting the largest ΔT from each of the quaternary families is presented in Figure 3.5.

Table 3.3: Thermodynamic data for quaternary variants of large ΔT ternary compositions obtained by substituting Cu for Be.

	T_g[C]	T_{x1}[C]	T_{x2}[C]	ΔT	ΔH_x (J/mol)	T_s[C]	T_L[C]	GFA
$Zr_{40}Ti_{25}Be_{35}$ (Alloy L)	300.2	409	429	108.8	5796	838	934.3	>1mm
$Zr_{40}Ti_{25}Be_{29}Cu_6$	306.5	454.9	-	148.4	7184	682.2	839.9	>10mm
$Zr_{40}Ti_{25}Be_{27}Cu_8$	306.2	464.3	-	158.1	7304	679.5	806.8	>10mm
$Zr_{40}Ti_{25}Be_{25}Cu_{10}$	306.2	470	-	163.8	6316	677.5	773.7	>10mm
$Zr_{40}Ti_{25}Be_{23}Cu_{12}$	308	389	464.5	81	9333	675.7	740.3	>10mm
$Zr_{27.5}Ti_{35}Be_{37.5}$ (Alloy P)	317.4	440.2	456.5	123	7167	832.7	843	>1mm
$Zr_{27.5}Ti_{35}Be_{29.5}Cu_8$	317.7	455.4	-	137.7	5707	669.7	834.3	>10mm
$Zr_{32.5}Ti_{30}Be_{37.5}$ (Alloy Q)	314.2	427.5	441.8	113.3	6469	836.8	846.8	>1mm
$Zr_{32.5}Ti_{30}Be_{31.5}Cu_6$	317.2	466.5	-	149.3	6976	673.1	>850	>10mm
$Zr_{32.5}Ti_{30}Be_{29.5}Cu_8$	314.5	471.9	-	157.4	8099	671.1	819.7	>10mm
$Zr_{32.5}Ti_{30}Be_{27.5}Cu_{10}$	314.6	474.2	-	159.6	8248	670.2	788	>10mm
$Zr_{32.5}Ti_{30}Be_{25.5}Cu_{12}$	317.1	409.1	456.2	92	7922	672.4	760.8	>10mm
$Zr_{37.5}Ti_{25}Be_{37.5}$ (Alloy R)	314.1	413.2	431.4	99.1	6800	831.1	857.7	>1mm
$Zr_{37.5}Ti_{25}Be_{27.5}Cu_{10}$	310.8	470.9	-	160.1	7349	674.7	807	>10mm
$Zr_{30}Ti_{30}Be_{40}$ (Alloy V)	330.1	447.4	-	117.3	6659	825.5	844.1	>1mm
$Zr_{30}Ti_{30}Be_{32}Cu_8$	318	462.8	-	144.8	6783	668.5	850	>1mm
$Zr_{30}Ti_{30}Be_{30}Cu_{10}$	322.8	467.2	-	144.4	5739	668.7	772.8	>10mm
$Zr_{30}Ti_{30}Be_{27.5}Cu_{12.5}$	323.1	442.7	-	119.6	7557	663.2	816.7	>10mm
$Zr_{35}Ti_{25}Be_{40}$ (AlloyW)	325.5	432.4	-	106.9	6422	836.5	850	>1mm
$Zr_{35}Ti_{25}Be_{32}Cu_8$	323.3	462.2	-	138.9	7825	676.4	748	>10mm
$Zr_{35}Ti_{25}Be_{30}Cu_{10}$	321.8	472.9	-	151.1	8101	675.3	716	>10mm
$Zr_{35}Ti_{25}Be_{28}Cu_{12}$	323.1	470.8	-	147.7	8225	673	711.4	>10mm
$Zr_{40}Ti_{20}Be_{40}$ (Alloy X)	324.8	415.9	-	91.1	6323	842.3	907.2	>1mm
$Zr_{40}Ti_{20}Be_{26.25}Cu_{13.75}$	316.3	467.6	-	151.3	7352	674.3	841.5	>10mm

Error bars are ± 3 °C on temperatures and ± 5% on ΔH_x.

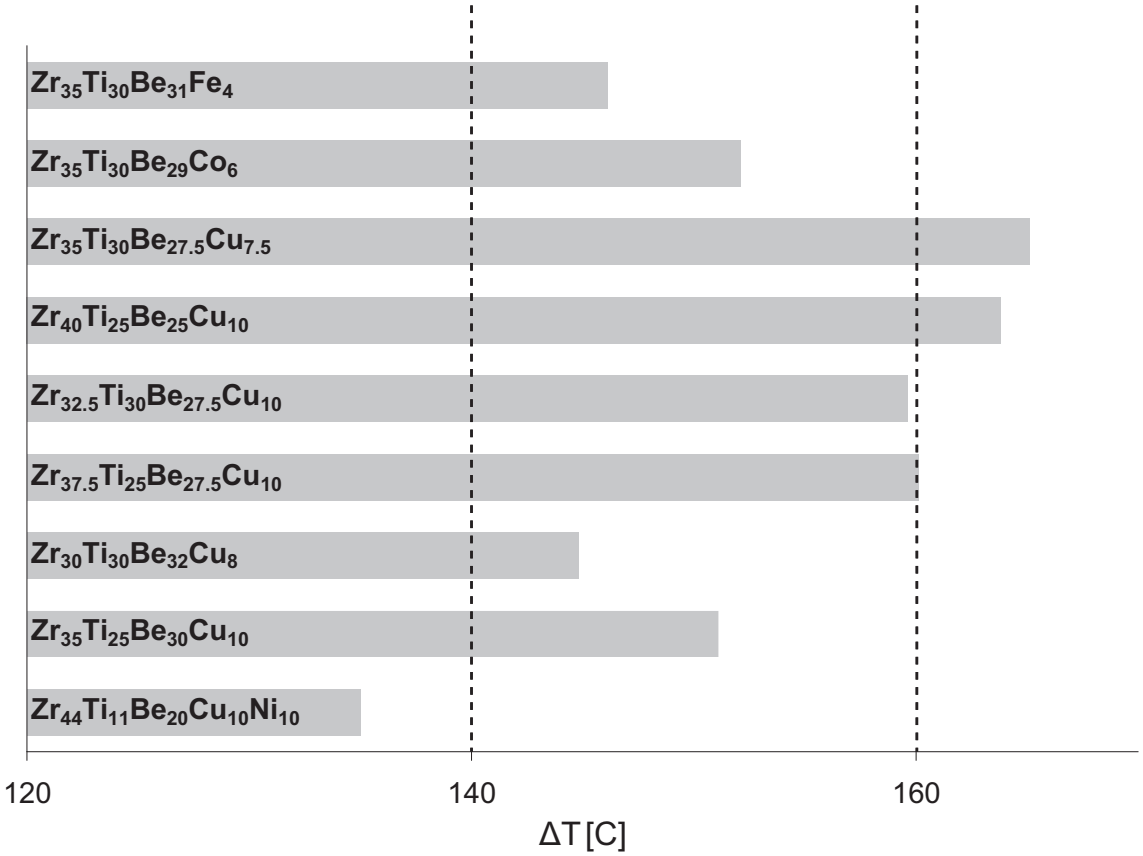

Figure 3.5: Bar graph showing the compositions with the largest ΔT from each quaternary family. Alloys with ΔT values as large as 165.1 °C are shown. $Zr_{44}Ti_{11}Be_{25}Cu_{10}Ni_{10}$ (Vitreloy 1b) is shown for reference.

3.4 Conclusion

An alloy development approach is presented, by which ZrTi based Be bearing bulk glass forming compositions were optimized for high thermal stability. From the optimization of the ternary ZrTiBe system, the following conclusions can be drawn:

- Several ternary bulk glass forming compositions were identified, capable of forming glasses with critical casting thicknesses exceeding 6mm.
- Several ternary glass forming compositions with thermal stabilities exceeding 120 °C were identified.

- The ternary alloys exhibiting good glass forming abilities and high thermal stabilities tend to undergo simultaneous or near-simultaneous crystal growth upon crystallization at 20 K/min heating rate.

The ternary alloy $Zr_{35}Ti_{30}Be_{35}$ was found to exhibit the best combination of glass forming ability and thermal stability, and was singled out for development of high thermal stability quaternary compositions. The following conclusions can be drawn from the optimization of the quaternary alloys:

- High thermal stability quaternary glasses with good glass forming ability were obtained by substituting small fractions of Be (4 - 10 atomic percent) with late transition metals such as Cu, Co, Fe, and Al.
- Cu substitution of Be is found to yield quaternary alloys with the best combination of thermal stability and glass forming ability. For example, $Zr_{35}Ti_{30}Be_{27.5}Cu_{7.5}$ is found to have a thermal stability exceeding 165 °C and a critical casting thickness greater than 15mm.
- The optimization strategy yielded twelve quaternary alloys with thermal stabilities >150 °C, three of which have thermal stabilities exceeding 160 °C.

Owing to the high thermal stability of their supercooled liquid states, these glasses are promising candidates for forming processes that can be performed thermoplastically in the SCLR. Furthermore, the high stability of the supercooled liquid states of these alloys will enable studies of liquid thermodynamics, rheology, atomic diffusion, and the glass transition to an extent previously not possible in metallic glass forming systems.

This alloy development strategy could be employed in other systems where ternary phase diagrams are known. Comparison of Figures 3.1 and 3.2 reveals that the

best glass formers in the ternary phase space were located near the lowest melting temperature region. Computer models designed to predict bulk glass forming compositions have enjoyed limited success to date. Perhaps the simplest approach would be to estimate ternary phase diagrams from known binary phase diagrams using a CALPHAD type approach and then check GFA of alloys near low melting temperature regions.

The authors thank the Office of Naval Research for their support of this work under ONR06-0566-22.

Chapter 3 References

[1] A.L. Greer, E. Ma, MRS Bull. 32 (2007) 611.
[2] W.L. Johnson, MRS Bull. 24 (1999) 42.
[3] A. Inoue, Acta Mater. 48 (2000) 279.
[4] W.L. Johnson, JOM 54 (2002) 40.
[5] J. Schroers, JOM 57 (2005) 35.
[6] B. Zhang, D.Q. Zhao, M.X. Pan, W.H. Wang, A.L. Greer, Phys. Rev. Lett. 94 (2005) 205502.
[7] C.A. Angell, J. Non-Cryst. Solids 131 (1991) 13.
[8] J. Schroers, Q. Pham, A.J. Desai, Micromech. Microeng. 16 (2007) 240.
[9] Y. Saotome, K. Imai, C. Shioda, S. Shimizu, T. Zhang, A. Inoue, Intermetallics 10 (2002) 1241.
[10] J. Degmova, S. Roth, J. Eckert, H. Grahl, L. Schultz, Mat. Sci. Eng. A 375 (2004) 265.
[11] K.S. Lee, Y.W. Chang, Mat. Sci. Eng. A 399 (2005) 238.
[12] J. Schroers, Q. Pham, A. Peker, N. Paton, R.V. Curtis, Scripta Mater. 57 (2007) 341.
[13] L.E. Tanner, R. Ray, Acta Metall. 27 (1979) 1727.
[14] R.G. Hennig, A.E. Carlsson, K.F. Kelton, C.L. Henley, Phys. Rev. B 71 (2005) 144103.
[15] B. Van de Moortele, T. Epicier, J.L. Soubeyroux, J.M. Pelletier, Philos. Mag. Lett. 84 (2004) 245.
[16] G. Duan, A. Wiest, M.L. Lind, J. Li, W.K. Rhim, W.L. Johnson, Adv. Mater. 19 (2007) 4272.
[17] L.E. Tanner, R. Ray, C.F. Cline, US Patent #4050931.
[18] L. Kaufman, L.E. Tanner, CALPHAD 3 (1979) 91.
[19] G. Duan, A. Wiest, M.L. Lind, A. Kahl, W.L. Johnson, Scripta Mater. 58 (2008) 465.
[20] A. Peker, W.L. Johnson, Appl. Phys. Lett. 63 (1993) 2342.